

Interplay of intrinsic disorder and macromolecular crowding on fibril formation of α -synuclein

Nobu C. Shirai¹ and Macoto Kikuchi^{2,3,4}

¹Graduate School of Science, Kyoto University, Sakyo, Kyoto 606-8502, Japan

²Cybermedia Center, Osaka University, Toyonaka, Osaka 560-0043, Japan

³Graduate School of Science, Osaka University, Toyonaka, Osaka 560-0043, Japan

⁴Graduate School of Frontier Biosciences, Osaka University, Suita, Osaka 565-0871, Japan

April 20, 2019

Abstract

α -synuclein (α -syn) is the intrinsically disordered protein which is considered to be one of the causes of Parkinson's disease. This protein forms amyloid fibrils when in a highly concentrated solution. The fibril formation of α -syn is induced not only by increases in α -syn concentration but also by macromolecular crowding. We focused on the relation between the intrinsic disorder of α -syn and macromolecular crowding, and constructed a simplified model of α -syn including crowding agents based on statistical mechanics. The main assumption was that α -syn can be expressed as coarse-grained particles with internal states coupled with effective volume; and disordered states were modeled by larger particles with larger internal entropy than other states. It was found that the crowding effect is taken into account as the effective internal entropy; and the crowding effect reduces the effective internal entropy of disordered states. From a Monte Carlo simulation, we provide scenarios of crowding-induced fibril formation. We also discuss the recent controversy over the existence of helically folded tetramers of α -syn, and suggest that macromolecular crowding is the key to resolving the controversy.

1 Introduction

α -synuclein (α -syn) is a 140-amino-acid protein [1] expressed in presynaptic terminals of the central nervous system [2, 3, 4, 5]. α -syn is known as an intrinsically disordered protein (IDP), which lacks secondary or tertiary structures [6, 7, 8]. Growing evidence suggests that α -syn has a causative role in Parkinson's disease (PD), which is the second most common neurodegenerative disease after Alzheimer's disease. Genetic mutations in α -syn (A30P, E46K and A53T) which have been identified in familial PD (FPD) directly link α -syn with PD [9, 10, 11, 12]. Duplication and triplication of the α -syn gene are also found in FPD [13, 14, 15]. The intracellular inclusions called Lewy bodies are the pathological hallmark of PD, and they are mainly composed of α -syn [16, 17]. Lewy bodies also link α -syn with PD. Furthermore, *in vitro* studies revealed that β -sheet-rich amyloid fibrils are formed in high-concentration α -syn solutions after hours or days of incubation [18, 19], and that introduction of these fibrils into cultured cells with overexpression of α -syn leads to the formation of Lewy body-like inclusions [20]. Inhibition of α -syn fibril formation is one of the suggested therapeutic approaches for PD [21, 22, 23, 24], and thus a good understanding of such fibril formation is needed.

Fibril formation of α -syn is a nucleation-dependent process [25]. Nucleation of α -syn protofibrils occurs above a certain α -syn concentration, which is called the critical concentration, and fibrils grow only after nucleation [18, 25, 19]. Kinetics of the fibril formation are affected by macromolecular crowding, and crowding agents induce and accelerate the fibril formation of α -syn [26, 27]. White et al. observed that fibril formation of IDPs including α -syn is accelerated and that of folded proteins is decelerated by macromolecular crowding, and they concluded that accelerated fibril formation is characteristic of IDPs [28]. Macromolecular crowding is an important factor in considering the fibril formation of α -syn.

In 2011, Bartels et al. reported the existence of helically folded tetramers of α -syn [22]. Although helically folded monomers of α -syn had already been identified as a lipid-bound form at that time [29, 30, 7, 31, 32, 33, 34], this was the first report of a tetrameric state of helically folded monomers. These tetramers resist amyloid fibril formation, and they suggested that stabilization of helically folded tetramers is one of the possible strategies for designing an amyloid inhibitor. There are three other reports which support the result of Bartels et al. [35, 36, 24]. The existence of helically folded tetramers is, however, still controversial; Fauvet et al. [23] and Burré et al. [37] concluded that α -syn exists predominantly as a disordered monomer. Fauvet et al. suggested that stabilization of a disordered monomer of α -syn can be an alternative strategy to inhibit fibril formation. We summarize the equilibrium state of α -syn including the tetrameric states in Fig. 1.

In this paper, we construct a highly simplified model of α -syn with crowding agents. Disordered states and fibril-forming β -sheet-rich states (β states) are assumed as internal states of α -syn. This model enables us to investigate the coupled effect of crowding and intrinsic disorder on fibril formation. We also investigate the thermal stability of helically folded tetramers by adding tetramer-forming α -helix-rich states (α states) to the internal states of α -syn.

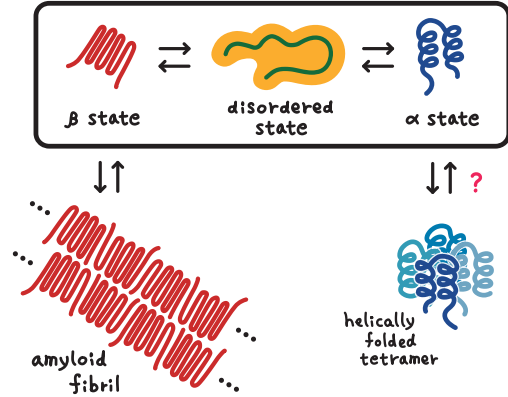


Figure 1: Equilibrium of α -synuclein. Monomeric α -synuclein (α -syn) is in equilibrium between three states: a β -sheet-rich state (β state), a disordered state and an α -helix-rich state (α state). α -syn aggregates into a β -sheet-rich amyloid fibril above a critical concentration. The existence of helically folded tetramer is still controversial.

2 Models

We constructed a model of α -syn using a two-dimensional lattice gas model. α -syns and crowding agents are modeled as particles on a lattice. The definitions of these molecules are shown in Fig. 2a. α -syn has three types of internal states: two β states (β_H and β_V), two disordered states (d_H and d_V) and four α states (α_{NE} , α_{SE} , α_{SW} and α_{NW}). The variations of each type of the states correspond to orientations of α -syn.

We assumed that the disordered states are larger than the other states based on the fact that disordered α -syn has a larger gyration radius than folded proteins with the same number of residues [6, 38, 39]. The disordered states occupy two sites and all the other states and crowding agents occupy a single site (Fig. 2a). We also assumed that the disordered states have internal entropy s based on the fact that α -syns exhibit significant entropy loss when they bind to a lipid bilayer surface and fold into an α -helical structure [40, 41]. We simply introduced the difference of entropy between disordered states and folded states by s .

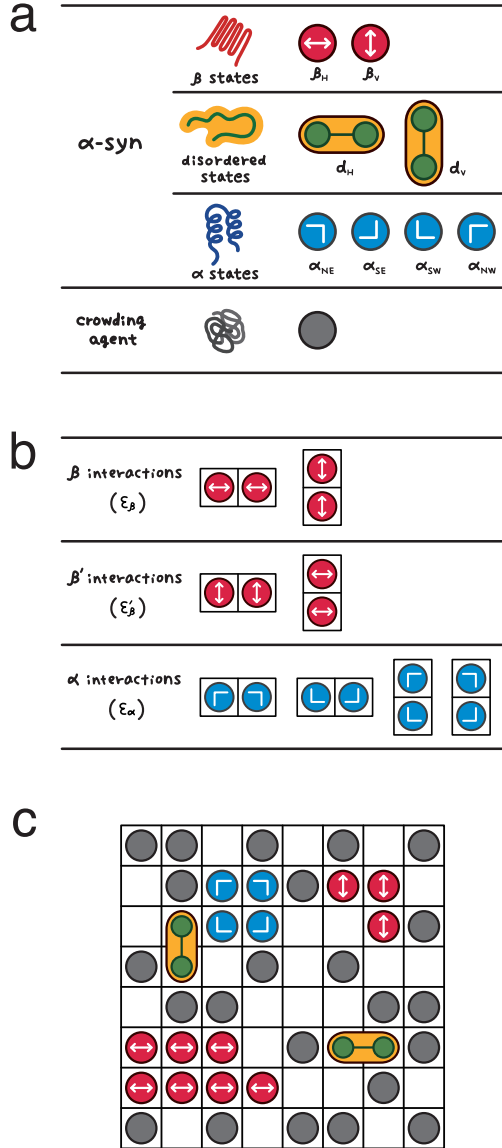


Figure 2: Lattice gas model of α -synuclein. (a) Definitions of two molecules. α -synuclein (α -syn) has three types of internal states: two β states (β_H and β_V), two disordered states (d_H and d_V) and four α states (α_{NE} , α_{SE} , α_{SW} and α_{NW}). The crowding agent has only one state. d_H and d_V occupy two sites while the other internal states of α -syn and the crowding agent occupy a single site. (b) There are three types of interactions between two α -syns at nearest-neighboring sites: two β interactions, two β' interactions and four α interactions. The interaction constants of these three interactions are given by ϵ_β , ϵ'_β and ϵ_α , respectively. (c) Snapshot of a small system ($L = 8, N = 16$) of the lattice gas model.

We defined two types of interactions between two β_H and two β_V based on the model of amyloid fibril formation given by Zhang and Muthukumar [42]. The definitions of these interactions are shown in Fig. 2b. Two horizontally-aligned β_H and two vertically-aligned β_V have β interactions. A linear chain of α -syns aligned by the β interactions defines the longitudinal direction of a fiber. Two β_H and two β_V have β' interactions in the direction perpendicular to the longitudinal one. The interaction constants of the β and β' interactions are given by ϵ_β and ϵ'_β ($\epsilon_\beta < 0, \epsilon'_\beta \leq 0, |\epsilon'_\beta| \leq |\epsilon_\beta|$), respectively.

We defined four α interactions between four pairs of α states, as shown in Fig. 2b. Dimers, trimers and tetramers of α states are formed by the α interactions. There are no conformations which include oligomers of α states larger than tetramers connected by the α interactions. The interaction constant of the α interactions is ϵ_α ($\epsilon_\alpha < 0$). Crowding agents do not have intermolecular interaction except excluded volume interaction.

We defined two models by including or excluding the internal states of α -syn: BD and BDA . The letters B , D and A correspond to β states, disordered states and α states, respectively. The BD model, for example, includes β states and disordered states. We also defined B^oD and B^oDA , which correspond to the BD and BDA models without β' interaction, as controls.

We considered a canonical ensemble of the four models presented above combined with a grand canonical ensemble of crowding agents. We defined a system by an $L \times L$ square lattice with N α -syns surrounded by walls in contact with a crowding agent reservoir at temperature T and chemical potential μ . μ controls the number of crowding agents, and the $\mu = -\infty$ system corresponds to the system without crowding agents. We defined a state of the system by a configuration of N α -syns with a determined internal state and m crowding agents on the lattice. We show a snapshot of a small system ($L = 8, N = 16$) of the BDA model in Fig. 2c, which includes all the internal states and all of the β and α interactions, as an example. A short fiber and a helically folded tetramer are also shown in the snapshot. The numbers of the internal states of α -syn n_β , n_d and n_α are

counted as $n_\beta = 10$, $n_d = 2$ and $n_\alpha = 4$ in the snapshot. The number of crowding agents is $m = 23$. The total energy E is calculated as $E = 6\varepsilon_\beta + 4\varepsilon'_\beta + 4\varepsilon_\alpha$.

The grand partition function of the N α -syn system is given by

$$\Xi = \sum_{E, n_d, m} W(E, n_d, m) e^{-\frac{E}{T}} e^{\sigma n_d} e^{\frac{\mu}{T} m}, \quad (1)$$

where $W(O_1, O_2, O_3, \dots)$ is the number of states of the system with physical quantities O_i ($i = 1, 2, 3, \dots$). We took the Boltzmann constant $k_B = 1$.

3 Metropolis method for the lattice gas model of α -synuclein including crowding agents

We used the Metropolis method to produce an equilibrium. In the lattice model of α -syn, a state of the system is given by conformations of N α -syns and m crowding agents on the $L \times L$ lattice. The transition probability from state i to state j is given by

$$p(i \rightarrow j) = \min \left[\frac{\exp(-E^j/T + \sigma n_d^j)}{\exp(-E^i/T + \sigma n_d^i)}, 1 \right]. \quad (2)$$

We defined the following four Monte Carlo moves for α -syns which are performed with the transition probability in Eq. 2.

- (i) Local displacement of a single α -syn: (a) If a selected α -syn is in a β or α state, move it in a randomly selected direction (north, south, east or west) by one site. This move will be rejected if the destination site is covered with another α -syn. (b) If a selected α -syn is in a disordered state, move it to a randomly selected direction by one site. This move will be rejected if one or both of the two destination sites are covered with other α -syns.
- (ii) Local displacement of a group of α -syns: (a) In the case that the selected α -syn is a part of a

β -state linear chain connected by β interactions, move the whole linear chain to a randomly selected direction by one site if the destination sites are empty. This move will be rejected if the number of β interactions increases. (b) In the case that the selected α -syn is a part of an α -state oligomer (dimer, trimer or tetramer) connected by α interactions, move the oligomer to a randomly selected direction by one site if the destination sites are empty. This move will be rejected if the number of α interactions increases. (c) In the case that a selected α -syn is not connected with other α -syns by β or α interaction, perform the move shown in (i), above. This move will be rejected if the number of β or α interactions increases.

- (iii) Nonlocal displacement of a single α -syn: (a) If a selected α -syn is in a β or α state, move it to a randomly selected site of the system. This move will be rejected if the destination site is covered with other α -syns. (b) If a selected α -syn is in a disordered state, move it to two randomly selected adjacent sites of the system. This move will be rejected if one or both of the two destination sites are covered with other α -syns.
- (iv) Internal state switching: Switch the internal state of a selected α -syn to another randomly selected state. This move will be rejected if a disordered state is selected as the next state and if it overlaps with another α -syn.

We randomly select an α -syn from the system, and randomly perform one of (i-iv) with prescribed probabilities. In all cases of (i), (ii) and (iii), the move will be rejected if the selected α -syns go outside the system.

4 Results

4.1 The effect of macromolecular crowding is taken into account as the effective internal entropy of disordered states

In the N α -syn system, there are $L^2 - N - n_d$ empty sites, and we can count configurations of m single-site crowding agents by the combination $\binom{L^2 - N - n_d}{m}$, where $0 \leq m \leq L^2 - N - n_d$. Using the identity

$$\sum_{m=0}^{L^2 - N - n_d} \binom{L^2 - N - n_d}{m} e^{\frac{\mu}{T} m} = \left(1 + e^{\frac{\mu}{T}}\right)^{L^2 - N - n_d},$$

we can rewrite the grand partition function in Eq. 1 as

$$\begin{aligned} \Xi &= \left(1 + e^{\frac{\mu}{T}}\right)^{L^2 - N} \sum_{E, n_d} w(E, n_d) e^{-\frac{E}{T}} e^{\sigma n_d} \\ &= \left(1 + e^{\frac{\mu}{T}}\right)^{L^2 - N} Z, \end{aligned} \quad (3)$$

where $w(O_1, O_2, O_3, \dots)$ is the number of states of the system with $m = 0$ and physical quantities O_i ($i = 1, 2, 3, \dots$), and we defined the effective entropy σ and the canonical partition Z as

$$\sigma = s - \log\left(1 + e^{\frac{\mu}{T}}\right), \quad (4)$$

$$Z = \sum_{E, n_d} w(E, n_d) e^{-\frac{E}{T}} e^{\sigma n_d}. \quad (5)$$

A thermal average of a physical quantity O is calculated as

$$\langle O \rangle = \frac{1}{\Xi} \sum_{O, E, n_d, m} O W(O, E, n_d, m) e^{-\frac{E}{T}} e^{\sigma n_d} e^{\frac{\mu}{T} m}. \quad (6)$$

In the case of $O = m$, Eq. 6 is written as

$$\begin{aligned} \langle m \rangle &= T \frac{\partial}{\partial \mu} \log \Xi \\ &= T \frac{\partial}{\partial \mu} \log \left(1 + e^{\frac{\mu}{T}}\right)^{L^2 - N} + T \frac{\partial}{\partial \mu} \log Z \\ &= \frac{1}{e^{-\frac{\mu}{T}} + 1} \left\{ L^2 - N - \langle n_d \rangle \right\}, \end{aligned} \quad (7)$$

using the Fermi distribution function $\frac{1}{e^{-\mu/T} + 1}$. If O is not a function of m , Eq. 6 is rewritten further using Z as

$$\langle O \rangle = \frac{1}{Z} \sum_{O, E, n_d} O w(O, E, n_d) e^{-\frac{E}{T}} e^{\sigma n_d}. \quad (8)$$

This means that the original ensemble with a single-site crowding agent reservoir is written as a canonical ensemble of an N α -syn system of which disordered states have the effective internal entropy σ . Thus, the effect of macromolecular crowding is absorbed in σ of disordered states.

In the limit of $\mu \rightarrow \infty$, that is, $\sigma \rightarrow -\infty$ from Eq. 4, Eq. 8 is rewritten as

$$\langle O \rangle = \frac{1}{Z} \sum_{O, E} O w(O, E) e^{-\frac{E}{T}}, \quad (9)$$

and the models with disordered states reduce to those without disordered states.

Note that the same analysis is also valid for three-dimensional lattice models as long as we consider single-site crowding agents.

4.2 Protofibril formation above the critical concentration of α -synuclein

We calculated thermal averages through a Monte Carlo simulation using the Metropolis method based on Eq. 5 and 8. We did not consider crowding agents explicitly in the simulation; instead we introduced σ calculated from Eq. 4 with a given μ . Details of the method are given in the Methods section. We use the following values throughout this paper: $L = 128$, $T = 1$, $\varepsilon_\beta = -8$, $\varepsilon'_\beta = -0.5$, $\varepsilon_\alpha = \varepsilon_\beta/1.2 \simeq -6.67$ and $s = 5$. We use N and μ as parameters.

In the simulations for the BD and BDA models, α -syns form a two-dimensional β -state cluster, which involves both β and β' interactions, above a certain N . We refer to the β -state cluster as a protofibril, and we write the critical value of N as N_c . For $N \simeq N_c$, we observe formation and dissolution of a protofibril repeatedly in equilibrium. For $N > N_c$, even if there are multiple protofibrils in the early stage of the

simulation, they merge into a single thermally stable protofibril. A protofibril is shown in Fig. 8, which is the snapshots of the BD model with $N = 1024$ and $\mu = 0$, as an example. In order to analyze protofibril formation, we define a β chain as a linear chain of β states connected by β interactions, and we define ℓ_β as the number of the β states in a β chain. If a β state is not connected with other α -syns by β interactions, we count ℓ_β as 1. We counted the number of β states in β chains of length ℓ_β for every ℓ_β .

N dependences of the $\langle n_\beta \rangle$ distributions for the BD and B^oD models with $\mu = 0$ are shown in Fig. 3a. The pairs of the curves of these models coincide for the $N = 512$ and 609 systems; they separate in the $N = 724$ and 861 systems, and the curves for the BD model have two peaks. The snapshots for the $N = 724$ and 861 systems of the BD model show that β chains with ℓ_β corresponding to the right peaks form a protofibril. We observed formation and dissolution of a protofibril in the BD model with $N = 724$, and thus N_c of the BD model is around 724.

N dependences of $\langle n_\beta \rangle$, $\langle n_\beta^{(f)} \rangle$, $\langle n_\beta^{(\bar{f})} \rangle$ and $\langle n_d \rangle$ for the BD and B^oD models with fixed μ are shown in the left column of Fig. 4. μ was set as $-\infty$, 0, 1, 2 and ∞ . Here, $n_\beta^{(f)}$ is the number of the β states connected to other β states by β' interactions, and $n_\beta^{(\bar{f})}$ is the number of the β states not connected to other β states by β' interactions. We counted the number of horizontally aligned β_V and vertically aligned β_H as $n_\beta^{(f)}$ also for the models without β' interactions. The sum of $n_\beta^{(f)}$ and $n_\beta^{(\bar{f})}$ is n_β , and thus $\langle n_\beta^{(f)} \rangle + \langle n_\beta^{(\bar{f})} \rangle = \langle n_\beta \rangle$. The sum of n_β and n_d is N in the BD and B^oD models, and thus $\langle n_\beta \rangle + \langle n_d \rangle = N$.

In all four graphs in the left column of Fig. 4, curves for the BD and B^oD models with the same μ separate at N_c except for $\mu = \infty$. The slopes of the $N - \langle n_\beta^{(f)} \rangle$ curves for the BD model change from ~ 0 to ~ 1 around N_c . Each $N - \langle n_\beta^{(\bar{f})} \rangle$ curve for the BD model has a maximum around N_c , and decreases to the constant value which does not depend on μ for large N . Each $N - \langle n_d \rangle$ curve for the BD model has a maximum around N_c , and decreases to a constant value. We found that N_c decreases as μ increases by comparing the separation points for different μ .

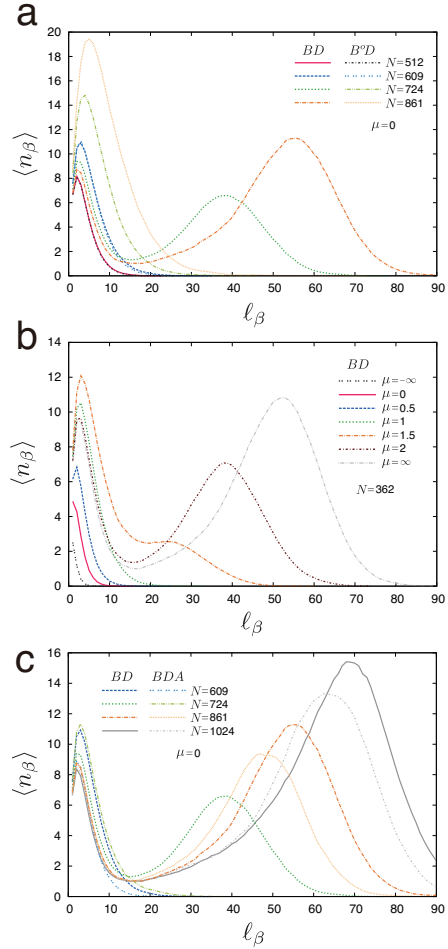


Figure 3: Equilibrium number of β states which are components of β chains of length ℓ_β . Here, we define a β chain as a linear chain of β states connected by β interactions. (a) N dependences of the $\langle n_\beta \rangle$ distributions against ℓ_β for the BD and B^oD models. (b) μ dependences of the $\langle n_\beta \rangle$ distributions against ℓ_β for the BD model. (c) N dependences of the $\langle n_\beta \rangle$ distributions against ℓ_β for the BD and BDA models.

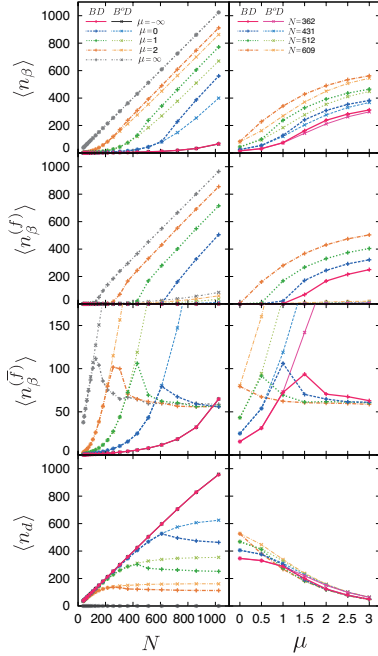


Figure 4: Left column: N dependences of $\langle n_\beta \rangle$, $\langle n_\beta^{(f)} \rangle$, $\langle n_\beta^{(\bar{f})} \rangle$ and $\langle n_d \rangle$ for the BD and B^oD models. Right column: μ dependences of $\langle n_\beta \rangle$, $\langle n_\beta^{(f)} \rangle$, $\langle n_\beta^{(\bar{f})} \rangle$ and $\langle n_d \rangle$ for the BD and B^oD models.

This means that macromolecular crowding reduces the critical concentration of α -syn.

4.3 Macromolecular crowding induces protofibril formation

μ dependences of the $\langle n_\beta \rangle$ distributions for the BD model with $N = 362$ are shown in Fig. 3b. As μ increases, the right peak begins to grow at $\mu = 1.5$, and gets larger at $\mu = 2$. We observed formation and dissolution of a protofibril in these systems, and thus the critical value of the chemical potential μ_c is around 1.5 for this N . This result suggests that macromolecular crowding induces protofibril formation, and this agrees with the experiments [26, 27].

μ dependences of $\langle n_\beta \rangle$, $\langle n_\beta^{(f)} \rangle$, $\langle n_\beta^{(\bar{f})} \rangle$ and $\langle n_d \rangle$ for the BD and B^oD models with fixed N are shown in

the right column of Fig. 4. N was set as 362, 431, 512 and 609. In all four graphs in the right column of Fig. 4, curves for the BD and B^oD models with the same N separate at μ_c . Each μ - $\langle n_\beta^{(\bar{f})} \rangle$ curve for the BD model has a maximum around μ_c , and decreases to the constant value which does not depend on N for large μ . The μ - $\langle n_d \rangle$ curves for both models monotonically decrease along with μ . Thus, macromolecular crowding reduces disordered states. Since $\langle n_\beta \rangle$ fulfills $\langle n_\beta \rangle = N - \langle n_d \rangle$, the μ - $\langle n_\beta \rangle$ curves for both models monotonically increase along with μ . Thus, macromolecular crowding promotes β states. We found that μ_c decreases as N increases by comparing the separation points for different values of N .

4.4 α -state tetramers suppress protofibril formation

N dependence of the ℓ_β - $\langle n_\beta \rangle$ curves for the BD and BDA models with $\mu = 0$ is shown in Fig. 3c. Although N_c for the BD model is about 724, the corresponding curve of the BDA model has only a single peak, and thus N_c is higher than that of the BD model. This means that introduction of α states raises N_c . Snapshots for the BD and BDA models of $N = 1024$ are shown in Fig. 8 and 9, respectively. A protofibril coexists with short β chains in both snapshots, and oligomers of α states are found in Fig. 9.

N and μ dependences of $\langle n_\beta \rangle$, $\langle n_\beta^{(f)} \rangle$, $\langle n_\beta^{(\bar{f})} \rangle$, $\langle n_d \rangle$, $\langle n_\alpha \rangle$, $\langle n_\alpha^{(t)} \rangle$ and $\langle n_\alpha^{(\bar{t})} \rangle$ are shown in the left and right columns of Fig. 5, respectively. Here, $\langle n_\alpha^{(t)} \rangle$ is the number of α states forming tetramers, and $\langle n_\alpha^{(\bar{t})} \rangle$ is the number of α states not forming tetramers. The sum of $n_\alpha^{(t)}$ and $n_\alpha^{(\bar{t})}$ is n_α , and thus $\langle n_\alpha^{(t)} \rangle + \langle n_\alpha^{(\bar{t})} \rangle = \langle n_\alpha \rangle$. The sum of n_β , n_α and n_d is N in the BDA and B^oDA models, and thus $\langle n_\beta \rangle + \langle n_\alpha \rangle + \langle n_d \rangle = N$.

We found that both N_c and μ_c decrease as μ increases by comparing the separation points. These behaviors are similar to those observed in the BD model. We also found that N_c and μ_c for the BDA model are larger than those for the BD model by comparing the separation points. This means that introduction of α states raises both the critical concentration of α -syn and the critical chemical potential

of crowding agents.

The overall shapes of the $N-\langle n_\beta \rangle$, $N-\langle n_\beta^{(f)} \rangle$, $N-\langle n_\beta^{(\bar{f})} \rangle$ and $N-\langle n_d \rangle$ curves in Fig. 5 are similar to those in Fig. 4. The $N-\langle n_\alpha \rangle$, $N-\langle n_\alpha^{(t)} \rangle$ and $N-\langle n_\alpha^{(\bar{t})} \rangle$ curves for the BDA and B^oDA models are all similar to the $N-\langle n_\beta^{(f)} \rangle$ curves. Each curve has a maximum around N_c , and decreases to the constant value which does not depend on μ . The majority of α states form tetramers around N_c , and thus we can say that α -state tetramers suppress fibril formation. This is consistent with the report of Bartels et al. [22]

5 Discussion

5.1 Scenario of protofibril formation induced by macromolecular crowding

The curves for the BD and BDA models in Fig. 4 and 5 are summarized in Fig. 6 as stacked graphs. N dependences are shown in the left, and μ dependences are shown in the right. The numbers of internal states fulfill $\langle n_\beta \rangle + \langle n_d \rangle = \langle n_\beta^{(f)} \rangle + \langle n_\beta^{(\bar{f})} \rangle + \langle n_d \rangle = N$ in the BD model, and they fulfill $\langle n_\beta \rangle + \langle n_\alpha \rangle + \langle n_d \rangle = \langle n_\beta^{(f)} \rangle + \langle n_\beta^{(\bar{f})} \rangle + \langle n_\alpha^{(t)} \rangle + \langle n_\alpha^{(\bar{t})} \rangle + \langle n_d \rangle = N$ in the BDA model. The $\langle n_\beta^{(f)} \rangle$ regions start to increase around N_c in the left graphs and μ_c in the right graphs, respectively. The existence of these critical values qualitatively agrees with the experiments of α -syn [18, 19, 26, 27].

$\langle n_\beta \rangle - \langle n_\beta^{(f)} \rangle$ and $\langle n_\beta \rangle - \langle n_\beta^{(\bar{f})} \rangle$ relations for all four models are plotted in Fig. 7a, and $\langle n_\beta \rangle - \langle n_\alpha \rangle$, $\langle n_\beta \rangle - \langle n_\alpha^{(t)} \rangle$ and $\langle n_\beta \rangle - \langle n_\alpha^{(\bar{t})} \rangle$ relations for the BDA and B^oDA models are plotted in Fig. 7b. These figures show that these relations do not depend on μ . Thus, the ratio of $\langle n_\beta \rangle$ to $\langle n_\alpha \rangle$ also does not depend on μ . We write the critical value of $\langle n_\beta \rangle$ as $\langle n_\beta \rangle_c$. Since $\langle n_d \rangle$ for the BD model with $\mu = \infty$ is zero for any N , and $\langle n_\beta \rangle$ is equal to N from the identity $\langle n_\beta \rangle + \langle n_d \rangle = N$, the graphs for the BD model with $\mu = \infty$ in Fig. 7a are exactly the same as those in Fig. 4. Thus, $\langle n_\beta \rangle_c$ of the BD and BDA models are

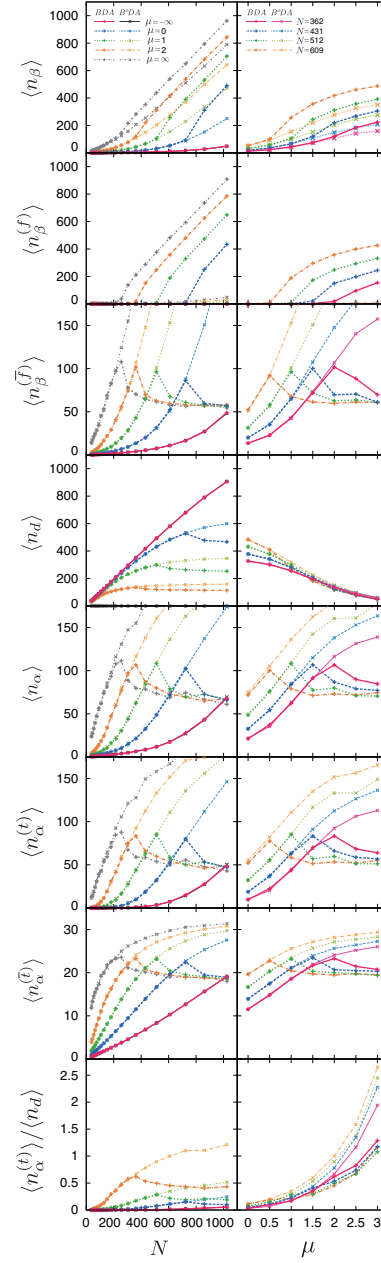


Figure 5: Left column: N dependences of $\langle n_\beta \rangle$, $\langle n_\beta^{(f)} \rangle$, $\langle n_\beta^{(\bar{f})} \rangle$, $\langle n_d \rangle$, $\langle n_\alpha \rangle$, $\langle n_\alpha^{(t)} \rangle$, $\langle n_\alpha^{(\bar{t})} \rangle$ and $\langle n_\alpha^{(t)} \rangle / \langle n_d \rangle$ for the BDA and B^oDA models. Right column: μ dependences of $\langle n_\beta \rangle$, $\langle n_\beta^{(f)} \rangle$, $\langle n_\beta^{(\bar{f})} \rangle$, $\langle n_d \rangle$, $\langle n_\alpha \rangle$, $\langle n_\alpha^{(t)} \rangle$, $\langle n_\alpha^{(\bar{t})} \rangle$ and $\langle n_\alpha^{(t)} \rangle / \langle n_d \rangle$ for the BDA and B^oDA models.

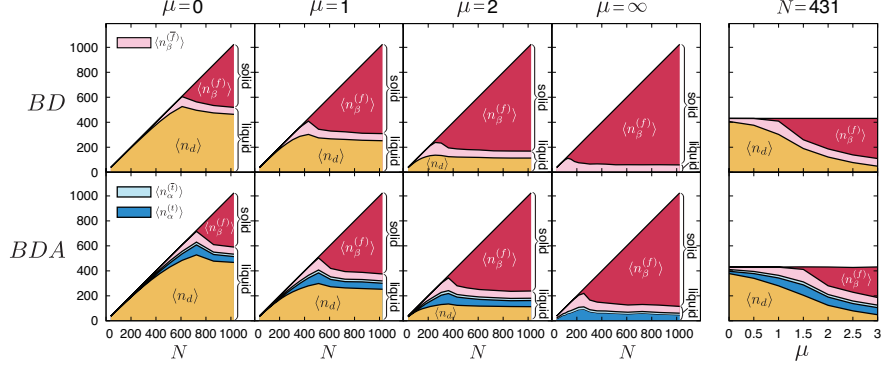


Figure 6: Stacked graphs of the equilibrium numbers of internal states for the BD and BDA models with $\mu = 0, 1, 2$ and ∞ , and $N = 431$. $\langle n_\beta^{(f)} \rangle$, $\langle n_\beta^{(\bar{f})} \rangle$, $\langle n_\alpha^{(\bar{t})} \rangle$, $\langle n_\alpha^{(t)} \rangle$ and $\langle n_d \rangle$ are colored red, pink, light blue, blue and yellow, respectively.

equal to N_c for the BD model with $\mu = \infty$ irrespective of μ .

We propose the following scenario for protofibril formation induced by macromolecular crowding based on the stacked graphs for μ dependence of internal states presented on the right of Fig. 6. (i) Since the stability of disordered states is determined by σ , which is given by Eq. 4, the $\langle n_d \rangle$ regions decrease along with μ as a result of decreasing σ . In other words, macromolecular crowding destabilizes the disordered states by reducing the effective internal entropy. (ii) As we explained above, the $\langle n_\beta \rangle$ region increases as a result of the decrease in $\langle n_d \rangle$ from $\langle n_\beta \rangle = N - \langle n_d \rangle$ in the BD model. In the case of the BDA model, the ratio of $\langle n_\beta \rangle$ and $\langle n_\alpha \rangle$ does not depend on μ , and thus we can write $\langle n_\beta \rangle \simeq k \langle n_\alpha \rangle$, ($k > 0$) irrespective of μ . Then, we can rewrite the identity $\langle n_\beta \rangle + \langle n_\alpha \rangle + \langle n_d \rangle = N$ as $\langle n_\beta \rangle \simeq \frac{1}{1+k} \{N - \langle n_d \rangle\}$. This also shows the increase in the $\langle n_\beta \rangle$ region as a result of the decrease in $\langle n_d \rangle$. (iii) If increased $\langle n_\beta \rangle$ is larger than $\langle n_\beta \rangle_c$, the $\langle n_\beta^{(f)} \rangle$ regions start to increase, and α -syns form a protofibril. At this point, $\mu \simeq \mu_c$. The factor $\frac{1}{1+k} (< 1)$ indicates that $\langle n_\beta \rangle$ of the BDA model is smaller than that of the BD model, and it explains why the μ_c of the BDA model is larger than that of the BD model.

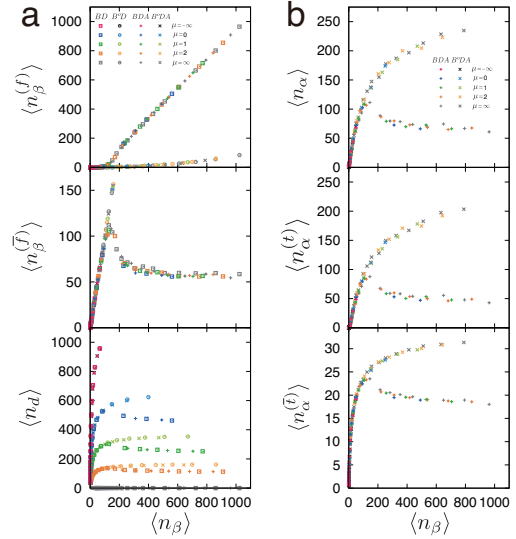


Figure 7: (a) $\langle n_\beta \rangle$ dependences of $\langle n_\beta^{(f)} \rangle$, $\langle n_\beta^{(\bar{f})} \rangle$ and $\langle n_d \rangle$ of the BD , B^oD , BDA and B^oDA models. (b) $\langle n_\beta \rangle$ dependences of $\langle n_\alpha \rangle$, $\langle n_\alpha^{(t)} \rangle$ and $\langle n_\alpha^{(\bar{t})} \rangle$ for the BD and B^oD models.

5.2 An explanation for the controversy over the observation of helically folded tetramers

We plotted the N and μ dependences of $\langle n_\alpha^{(t)} \rangle / \langle n_d \rangle$ for the BDA and B^oDA models at the bottom left and right of Fig. 5, respectively. Each N - $\langle n_\alpha^{(t)} \rangle / \langle n_d \rangle$ curve for the BDA model has a maximum around N_c , and decreases to a constant value. This means that relative stability of helically folded tetramers depends on the concentration of α -syn. The μ - $\langle n_\alpha^{(t)} \rangle / \langle n_d \rangle$ curves for the BDA model monotonically increase along with μ . Thus, macromolecular crowding increases the relative number of helically folded tetramers to that of disordered monomers. The macromolecular crowding effect may provide a good explanation for the controversy over the existence of helically folded tetramers. The present result that the density of such tetramers depends on crowdedness suggests that whether or not the tetramers are observed in experiments is determined by the crowdedness of the environment.

5.3 Solid–liquid equilibrium analogy

The left graphs in Fig. 6 show that $\langle n_\beta^{(f)} \rangle$ monotonically increases above N_c , while $\langle n_\beta^{(\bar{f})} \rangle$, $\langle n_d \rangle$, $\langle n_\alpha^{(t)} \rangle$ and $\langle n_\alpha^{(\bar{t})} \rangle$ each decrease to constant values. In other words, the protofibril absorbs increased α -syns above N_c while the other non-protofibril components converge to a constant concentration. From this result, we can draw an analogy of protofibril–non-protofibril equilibrium with a solid–liquid equilibrium; the protofibril can be seen as solid, and the non-protofibril components can be seen as liquid. The words “solid” and “liquid” are written in the stacked graphs.

5.4 A coarse-grained model with internal states: funnel gas model

The definition of disordered states and the derivation of Eq. 4 and 5 are applicable to other IDPs as long as the volume of folded states is greater than or equal to that of crowding agents. Eq. 4 and 5 will be a

first approximation to discuss the relation between macromolecular crowding and the stability of disordered states also for larger crowding agents. Eq. 4 provides a simple theoretical expression for the interplay of intrinsic disorder and macromolecular crowding which was suggested by White et al. [28].

The main assumption of our model is that proteins can be expressed as coarse-grained particles with some internal states coupled with the effective volume of each state. This simplification enables us to derive the expression of effective internal entropy shown above. Here, we generalize this idea. Proteins have a funnel-like energy landscape [43, 44, 45]. IDPs with a folded state in their bound complex with other proteins including α -syn also have a funnel-like energy landscape [46, 47]. In this study, we assumed that α -syn has a triple-well free-energy landscape, and we constructed the coarse-grained particle with the three internal states based on the free-energy landscape of α -syn. In the same way, we can also construct coarse-grained particles with internal states based on the free-energy landscape of specific proteins. Then, we can produce equilibrium states of multiple molecular systems including the crowding effect. This is the spirit of the new coarse-grained model, and we call this model the “funnel gas model”.

6 Acknowledgments

This work was supported by a Grant-in-Aid (Grant No. 21113006) from MEXT Japan, and the Global COE Program Core Research and Engineering of Advanced Materials-Interdisciplinary Education Center for Materials Science from MEXT Japan.

References

- [1] Uéda K et al. (1993) Molecular cloning of cDNA encoding an unrecognized component of amyloid in Alzheimer disease. *Proc Natl Acad Sci USA* 90:11282–11286.
- [2] Jakes R, Spillantini MG, Goedert M (1994) Identification of two distinct synucleins from human brain. *FEBS Lett* 345:27–32.

- [3] Iwai A et al. (1995) The precursor protein of non-A beta component of Alzheimer's disease amyloid is a presynaptic protein of the central nervous system. *Neuron* 14:467–475.
- [4] Kahle PJ et al. (2000) Subcellular Localization of Wild-Type and Parkinson's Disease-Associated Mutant α -Synuclein in Human and Transgenic Mouse Brain. *J Neurosci* 20:6365–6373.
- [5] Liu G et al. (2009) α -Synuclein is differentially expressed in mitochondria from different rat brain regions and dose-dependently down-regulates complex I activity. *Neuroscience Lett* 454:187–192.
- [6] Weinreb PH, Zhen W, Poon AW, Conway KA, Lansbury PT (1996) NACP, a protein implicated in Alzheimer's disease and learning, is natively unfolded. *Biochemistry* 35:13709–13715.
- [7] Eliezer D, Kutluay E, Bussell R, Browne G (2001) Conformational properties of α -synuclein in its free and lipid-associated states. *J Mol Biol* 307:1061–1073.
- [8] Uversky VN, Oldfield CJ, Dunker AK (2008) Intrinsically Disordered Proteins in Human Diseases: Introducing the D2 Concept. *Annu Rev Biophys* 37:215–246.
- [9] Kruger R et al. (1998) Ala30Pro mutation in the gene encoding α -synuclein in Parkinson's disease. *Nat Genet* 18:106–108.
- [10] Zarranz JJ et al. (2004) The new mutation, E46K, of α -synuclein causes parkinson and Lewy body dementia. *Ann Neurol* 55:164–173.
- [11] Polymeropoulos MH et al. (1997) Mutation in the α -Synuclein Gene Identified in Families with Parkinson's Disease. *Science* 276:2045–2047.
- [12] Muñoz E et al. (1997) Identification of Spanish familial Parkinson's disease and screening for the Ala53Thr mutation of the α -synuclein gene in early onset patients. *Neurosci Lett* 235:57–60.
- [13] Chartier-Harlin MCC et al. (2004) Alpha-synuclein locus duplication as a cause of familial Parkinson's disease. *Lancet* 364:1167–1169.
- [14] Ibáñez P et al. (2004) Causal relation between α -synuclein locus duplication as a cause of familial Parkinson's disease. *Lancet North Am Ed* 364:1169–1171.
- [15] Singleton AB et al. (2003) α -Synuclein locus triplication causes Parkinson's disease. *Science* 302:841.
- [16] Spillantini MG et al. (1997) α -Synuclein in Lewy bodies. *Nature* 388:839–840.
- [17] Spillantini MG, Crowther RA, Jakes R, Hasegawa M, Goedert M (1998) α -Synuclein in filamentous inclusions of Lewy bodies from Parkinson's disease and dementia with Lewy bodies. *Proc Natl Acad Sci USA* 95:6469–6473.
- [18] Hashimoto M et al. (1998) Human recombinant NACP/ α -synuclein is aggregated and fibrillated in vitro: Relevance for Lewy body disease. *Brain Res* 799:301–306.
- [19] van Raaij ME, van Gestel J, Segers-Nolten IMJ, de Leeuw SW, Subramaniam V (2008) Concentration Dependence of α -Synuclein Fibril Length Assessed by Quantitative Atomic Force Microscopy and Statistical-Mechanical Theory. *Biophys J* 95:4871–4878.
- [20] Luk KC et al. (2009) Exogenous α -synuclein fibrils seed the formation of Lewy body-like intracellular inclusions in cultured cells. *Proc Natl Acad Sci USA* 106:20051–20056.
- [21] Lashuel HA, Overk CR, Oueslati A, Masliah E (2013) The many faces of α -synuclein: from structure and toxicity to therapeutic target. *Nat Rev Neurosci* 14:38–48.
- [22] Bartels T, Choi JG, Selkoe DJ (2011) α -Synuclein occurs physiologically as a helically folded tetramer that resists aggregation. *Nature* 477:107–110.

- [23] Fauvet B et al. (2012) α -Synuclein in Central Nervous System and from Erythrocytes, Mammalian Cells, and Escherichia coli Exists Predominantly as Disordered Monomer. *J Biol Chem* 287:15345–15364.
- [24] Gould N et al. (2014) Evidence of Native α -Synuclein Conformers in the Human Brain. *J Biol Chem* 289:7929–7934.
- [25] Wood SJ et al. (1999) α -Synuclein Fibrillogenesis Is Nucleation-dependent. *J Biol Chem* 274:19509–19512.
- [26] Shtilerman MD, Ding TT, Lansbury PT (2002) Molecular Crowding Accelerates Fibrillization of α -Synuclein: Could an Increase in the Cytoplasmic Protein Concentration Induce Parkinson’s Disease?. *Biochemistry* 41:3855–3860.
- [27] Uversky VN, Cooper, Bower KS, Li J, Fink AL (2002) Accelerated α -synuclein fibrillation in crowded milieu. *FEBS Lett* 515:99–103.
- [28] White DA, Buell AK, Knowles TPJ, Welland ME, Dobson CM (2010) Protein Aggregation in Crowded Environments. *J Am Chem Soc* 132:5170–5175.
- [29] Davidson WS, Jonas A, Clayton DF, George JM (1998) Stabilization of α -Synuclein Secondary Structure upon Binding to Synthetic Membranes. *J Biol Chem* 273:9443–9449.
- [30] Jensen PH, Nielsen MS, Jakes R, Dotti CG, Goedert M (1998) Binding of α -synuclein to brain vesicles is abolished by familial Parkinson’s disease mutation. *J Biol Chem* 273:26292–26294.
- [31] Jao CC, Der-Sarkissian A, Chen J, Langen R (2004) Structure of membrane-bound α -synuclein studied by site-directed spin labeling. *Proc Natl Acad Sci USA* 101:8331–8336.
- [32] Jao CC, Hegde BG, Chen J, Haworth IS, Langen R (2008) Structure of membrane-bound α -synuclein from site-directed spin labeling and computational refinement. *Proc Natl Acad Sci USA* 105:19666–19671.
- [33] Ulmer TS, Bax A, Cole NB, Nussbaum RL (2005) Structure and Dynamics of Micelle-bound Human α -Synuclein. *J Biol Chem* 280:9595–9603.
- [34] Rao JN, Jao CC, Hegde BG, Langen R, Ulmer TS (2010) A Combinatorial NMR and EPR Approach for Evaluating the Structural Ensemble of Partially Folded Proteins. *J Am Chem Soc* 132:8657–8668.
- [35] Wang W et al. (2011) A soluble α -synuclein construct forms a dynamic tetramer. *Proc Natl Acad Sci USA* 108:17797–17802.
- [36] Dettmer U, Newman AJ, Luth ES, Bartels T, Selkoe D (2013) In Vivo Cross-linking Reveals Principally Oligomeric Forms of α -Synuclein and β -Synuclein in Neurons and Non-neural Cells. *J Biol Chem* 288:6371–6385.
- [37] Burre J et al. (2013) Properties of native brain α -synuclein. *Nature* 498:E4–E6.
- [38] Kim TD, Paik SR, Yang CH (2002) Structural and Functional Implications of C-Terminal Regions of α -Synuclein. *Biochemistry* 41:13782–13790.
- [39] Uversky VN, Li J, Fink AL (2001) Evidence for a Partially Folded Intermediate in α -Synuclein Fibril Formation. *J Biol Chem* 276:10737–10744.
- [40] Nuscher B et al. (2004) α -Synuclein Has a High Affinity for Packing Defects in a Bilayer Membrane. *J Biol Chem* 279:21966–21975.
- [41] Bartels T et al. (2010) The N-Terminus of the Intrinsically Disordered Protein α -Synuclein Triggers Membrane Binding and Helix Folding. *Biophys J* 99:2116–2124.
- [42] Zhang J, Muthukumar M (2009) Simulations of nucleation and elongation of amyloid fibrils. *J Chem Phys* 130:035102+.
- [43] Onuchic JN, Schulten ZL, Wolynes PG (1997) THEORY OF PROTEIN FOLDING: The Energy Landscape Perspective. *Annu Rev Phys Chem* 48:545–600.

- [44] Dill KA, Chan HS (1997) From Levinthal to pathways to funnels. *Nat Struct Biol* 4:10–19.
- [45] Go N (1983) Theoretical Studies of Protein Folding. *Annu Rev Biophys Bioeng* 12:183–210.
- [46] Shoemaker BA, Portman JJ, Wolynes PG (2000) Speeding molecular recognition by using the folding funnel: the fly-casting mechanism. *Proc Natl Acad Sci USA* 97:8868–8873.
- [47] Shirai NC, Kikuchi M (2013) Structural flexibility of intrinsically disordered proteins induces stepwise target recognition. *J Chem Phys* 139:225103+.

A Method of adding crowding agents to the snapshots produced by the simulation without explicit crowding agents

We explain the method of adding crowding agents based on μ to the snapshots produced by the method shown above. Here, we also use the Metropolis method to produce grand canonical ensemble of crowding agents. The transition probability from state i to state j is given by

$$p(i \rightarrow j) = \min \left[\frac{\exp(\mu m^j / T)}{\exp(\mu m^i / T)}, 1 \right]. \quad (10)$$

We randomly select a site from the system and perform the move shown below.

- Insertion or removal of a crowding agent: (a) In the case that a selected site is empty, insert a new crowding agent into that site. (b) In the case that a selected site is covered by a crowding agent, remove it from the system. (c) In the case that a selected site is covered by an α -syn, this move will be rejected.

When we created the snapshots shown in Fig. 8 and 9, we first created the snapshots by the simulation without explicit crowding agents, and then we added crowding agents to the snapshots by using the method presented here.

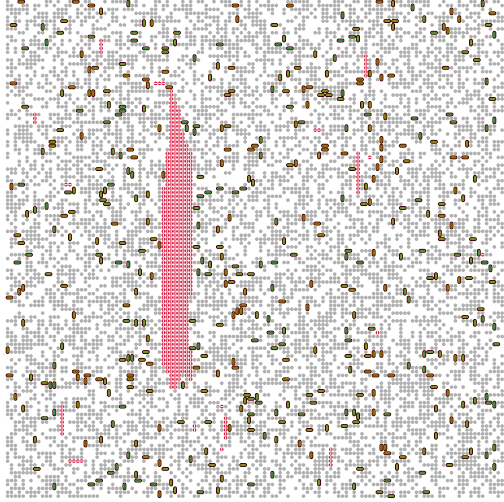


Figure 8: Snapshot for the BD model with $N = 1024$ and $\mu = 0$.

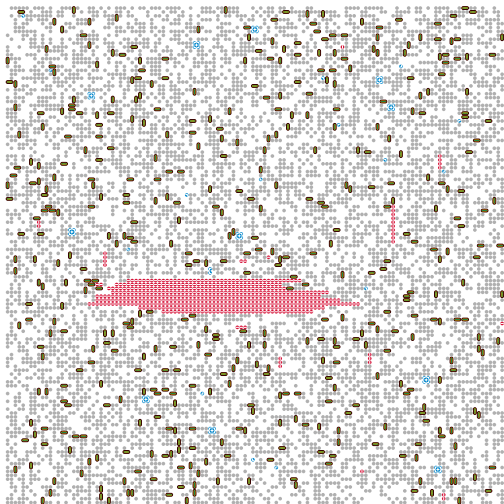


Figure 9: Snapshot for the BDA model with $N = 1024$ and $\mu = 0$.